

## Magnetostriction-driven multiferroicity of MnTe and MnTe/ZnTe epitaxial films

Helen V. Gomony and Ievgenia G. Komiienko

National Technical University of Ukraine "KPI", ave Peremogy, 37, 03056 Kyiv, Ukraine

(dated: September 8, 2024)

Here we demonstrate that MnTe epitaxial films with zinc-blend structure and MnTe/ZnTe multilayers should show ferroelectric polarization in antiferromagnetically (AFM) ordered state and thus belong to multiferroics. Spontaneous ferroelectric polarization results from the bending of highly ionic Mn-Te-Mn bonds induced by magnetostrictive shear strain. Orientation of ferroelectric polarization is coupled with orientation of AFM vector and thus can be controlled by application of the external magnetic field. Due to the clamping of electric and magnetic order parameters, domain structure in MnTe is governed by two mechanisms: depolarizing field produced by electric dipoles and destressing field produced by magnetoelastic dipoles. The values of monodomainization electric and magnetic fields depend upon the sample shape and diminish with the film thickness. Magnetoelastic nature of the domains make it possible to visualize the domain structure by linear and nonlinear optical methods (Kerr effect, second harmonic generation technique).

PACS numbers: 75.50.Ee Antiferromagnetics 75.50.Pp Magnetic semiconductors 75.80.+q Magnetomechanical and magnetoelastic effects, magnetostriction 77.80.-e Ferroelectricity and antiferroelectricity

## I. INTRODUCTION

Multiferroics are a class of a single phase or composite materials with coexisting magnetic and ferroelectric ordering. High susceptibility of multiferroics to both electric and magnetic fields which enables electrical control of magnetic state and vice versa makes them interesting from fundamental and applied points of view.

Some of multiferroics are ferroelectric and ferromagnetic (see, e.g., Refs. 1,2,3) and could be used as a storage media with high information capacity or as functionalized materials for electronic devices. Others (mainly rare earth compounds with Mn ions like  $\text{RMnO}_3$  or  $\text{RMn}_2\text{O}_5$ , where  $R = \text{Tb, Dy, Ho, Y, etc.}$ ) show ferroelectric and antiferromagnetic ordering<sup>4,5,6,7,8</sup> and may find an application as mediators for indirect electric control of ferromagnetic state of an adjacent layer.<sup>9</sup>

Cross-coupling between the magnetic and ferroelectric properties may be caused by different mechanisms. In type-I multiferroics (according to classification proposed in the recent review<sup>10</sup>) ferroelectricity and magnetism have different origin and coexist only in a certain temperature range. Materials classified as type-II show ferroelectricity only in a magnetically ordered state. Until now such a combined ferroelectric-magnetic ordering was observed in crystals which possess at least small noncompensated magnetization, i.e. in ferro-, ferri- and weak ferromagnets (see, for example, Refs. 4,11,12,13, etc.).

Two microscopic mechanisms of the magnetically-induced ferroelectricity originate from the exchange interactions<sup>4</sup>, namely, i) anisotropic exchange<sup>15,16</sup> (Dzyaloshinskii-Moriya interaction, DMI) and ii) exchange striction<sup>17</sup> (magnetoelastic coupling to the lattice). In the first case antisymmetric DMI activated by noncollinear spin ordering breaks inversion symmetry and induces electric polarization through the concomitant lattice and electronic distortion. Some typical examples of the compounds which show DMI are listed in Table I.

The second mechanism may play the dominant role in the antiferromagnets with superexchange interactions between the magnetic ions mediated by bridging via nonmagnetic anions, like  $\text{DyMn}_2\text{O}_5$  and  $\text{YMn}_2\text{O}_5$ , see Table I. In this case the value of exchange integral strongly depends upon an angle between anion-cation bonds. In the crystals with the competing antiferromagnetic (AFM) interactions even small bond-bending may reduce the exchange energy, stabilizes long-range AFM ordering and produce nonzero electric polarization.

In the present paper we predict multiferroicity caused by magnetoelastic mechanism in the epitaxially grown MnTe/ZnTe films and heterostructures that belong to the family of II-VI semiconductors<sup>18</sup> well suited to many optoelectronic applications in the infrared and visible range<sup>19</sup>. Our hypothesis is based on the following facts.

1. Epitaxial layers of MnTe, ZnTe, CdTe and corresponding heterostructures possess zinc-blend (ZB) structure consistent with piezoelectric activity. In particular, isomorphous to MnTe nonmagnetic films of ZnTe, CdTe, ZnTe/CdTe(111) can produce a macroscopic electric polarization when stressed or strained<sup>20</sup>.
2. Predominant mechanism of the magnetic interactions between  $\text{Mn}^{2+}$  ions is superexchange via Te anions<sup>18,21,22</sup> that favours antiferromagnetic ordering and noticeably varies with Mn-Te-Mn bond bending.
3. Magnetoelastic coupling in MnTe is rather strong as can be deduced from step-wise variation of lattice parameters at the Neel temperature.<sup>23,24</sup>
4. MnTe is a wide-gap (band gap is 3.2 eV, as reported in Ref. 18) semiconductor with vanishingly small concentration of the mobile carriers at low temperatures.<sup>25</sup> Thus, ferroelectric polarization should not be seriously affected by screening by

the mobile charge. In MnTe/ZnTe heterostructures such a screening can be avoided by a proper choice of the superlattice parameters and/or by doping.

We argue that the value of spontaneous ferroelectric polarization in MnTe can be as large as  $60 \text{ nC/cm}^2$  and thus is comparable with polarization of many other antiferromagnets (see Table I). Moreover, due to the direct coupling between magnetic and ferroelectric ordering, one should expect strong magnetoelectric effects (i.e., induction of polarization by a magnetic field) in this material. Magnetoelastic mechanism is responsible also for the nonlinear optical effects and opens a possibility to visualize antiferromagnetic (and corresponding ferroelectric) domains by use of second harmonic generation (SHG) technique (see, e.g, Refs. 26,27).

The paper is organized as follows. In Sec. II we describe crystal and magnetic structure of MnTe/ZnTe films and in Sec. III give some intuitive reasons for appearance of spontaneous electric polarization below the Neel point. In Sec. IV we calculate the value of spontaneous polarization on the basis of phenomenological model. Sec. V is devoted to the discussion of AFM and ferroelectric domains and methods of the domain structure control. In Sec. VI we discuss possible magneto-optical effects that could be helpful in visualization of the magnetic and ferroelectric structure of MnTe. In the last Sec. the summary of the results obtained is given.

## II. STRUCTURE AND MAGNETIC PROPERTIES OF MNTE

Bulk-like films of paramagnetic MnTe grown by MBE technique have zinc-blend structure<sup>35</sup> shown in Fig. 1 (symmetry group is  $F43m$ ). The direct exchange interaction between the nearest localized  $Mn^{2+}$  spins ( $S = 5/2$ ) is accomplished via Mn-Te-Mn bonds<sup>21</sup> and thus is antiferromagnetic. In the strain-free fcc lattice AFM exchange between the nearest neighbors (NN) is frustrated. Nevertheless, neutron diffraction experiments<sup>23,35</sup> reveal appearance of the long-range AFM type-III structure below the Neel temperature ( $T_N = 65 \text{ K}$ ). As shown in Fig. 2, this spin arrangement consists of AFM sheets parallel to (001) plane (represented in the plot by the shaded parallelograms). Stabilization of long-range ordering is attributed to the influence of weak NNN coupling<sup>23</sup> and to misfit-induced strain of the magnetic layer<sup>36</sup> which in the case of MnTe/ZnTe corresponds to elongation<sup>23</sup> ( $c/a = 1.06$ ) in the direction of film growth.

It should be noted that in the described AFM-III structure the coupling energy between the spins in the adjacent (001) sheets sums to zero, so, mutual rotation of spins in different layers does not change the energy of exchange interactions<sup>48</sup>. Stabilization of the collinear AFM-III structure can be due to the pronounced magnetostriction<sup>23</sup> (0.3%) that removes degeneracy between [100] and [010] directions within the film plane.

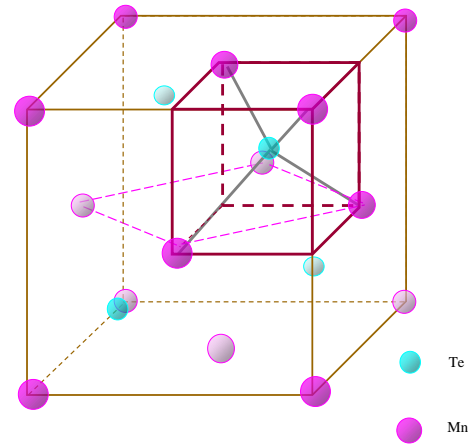


Figure 1: (Color online) Structure of zinc-blend MnTe. Mn - magenta (large) spheres, Te - blue (small) spheres. Inset (small cube) shows orientation of Mn-Te bonds.

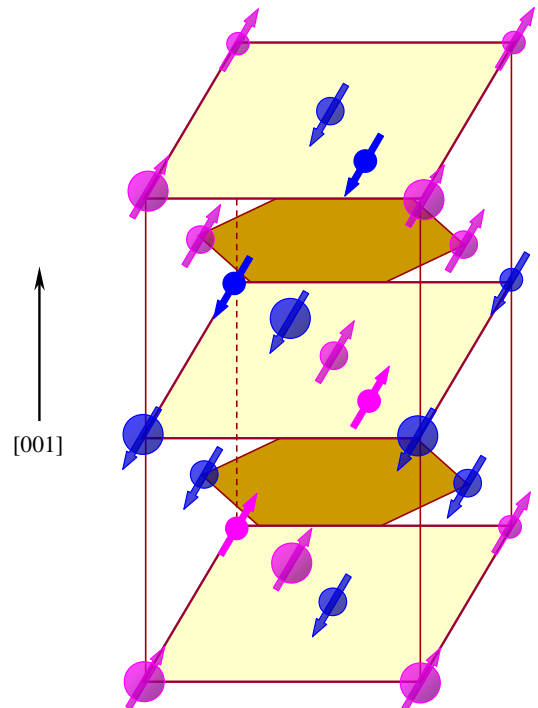


Figure 2: (Color online) Collinear AFM-III structure in the tetragonally distorted fcc spin lattice. Film growth direction is parallel to [001] crystallographic axis.  $Mn^{2+}$  ions with opposite spin direction are shown in different colours (opposite arrows).

It should be also mentioned that the symmetry of AFM state (corresponding group is generated by the rotation  $2_{[001]}$  and translation  $[\frac{1}{2}, \frac{1}{2}, 0]$  both combined with time inversion  $1^0$ ) allows the existence of macroscopic electric polarization vector oriented along the [001] axis and forbids existence of macroscopic magnetization.

Table I: Values of spontaneous electric polarization,  $P^{(\text{sp on})}$ , Neel temperature,  $T_N$ , type of AFM ordering (MO), microscopic mechanism and type (according to classification Ref.10) of ferroelectricity for some multiferroics (MF).

Compound	$P^{(\text{sp on})}$ (nC/cm <sup>2</sup> )	$T_N$ (K)	Type of MO	Mechanism	Type of MF	Source
BiFeO <sub>3</sub>	$12 \cdot 10^4$	673	cycloid	octahedra rot.	I	Ref.9
BiSrFeO <sub>3</sub>	$10 \cdot 10^4$	643	noncollinear	DMI	I	Ref.28
DyMn <sub>2</sub> O <sub>5</sub>	150	39	noncollinear	ME	II	Ref.29,30
YMn <sub>2</sub> O <sub>5</sub>	100	45	collinear	ME	II	Ref.17
MnTe (ZB)	60	65	collinear	ME	II	this work
TbMnO <sub>3</sub>	50	27	spiral	DMI	II	Ref.31
TbMn <sub>2</sub> O <sub>5</sub>	40	37	noncollinear	DMI	II	Ref.8
Ni <sub>3</sub> V <sub>2</sub> O <sub>8</sub>	12.5	6.3	noncollinear	DMI	II	Ref.32,33
MnWO <sub>4</sub>	4	12.7	noncollinear	DMI	II	Ref.7
Ca <sub>3</sub> CoMnO <sub>6</sub>	-	13	collinear, Ising	ME	II	Ref.34

### III. MULTIFERROICITY INDUCED BY MAGNETOSTRICTION: INTUITIVE CONSIDERATIONS

The role of magnetoelastic coupling in the formation of AFM-III structure can be traced from the following qualitative considerations. It was already mentioned that the value of Mn-Te-Mn angle is the key quantity in determining the exchange coupling constant  $J_{dd}$  between the NN Mn<sup>2+</sup> ions: upon decreasing the strength of AFM interaction increases. For small deviation from an ideal  $\theta_0 = 109.5^\circ$  angle peculiar to fcc lattice, this dependence can be approximated as follows (from the results of Bruno and Lascaray<sup>37</sup>)

$$J_{dd}(\theta) = 3.45 + 0.135(\theta - \theta_0); \text{ K} \quad (1)$$

Now, let us turn to Fig. 3 which illustrates the effect of tetragonal strain induced by the presence of ZnTe layers. In a nondeformed cubic lattice all the bonds make an "ideal" angle  $\theta_0$  and all NN interactions are equivalent. Tetragonal distortion in [001] direction removes degeneracy between in-plane (001) and interplane NN exchange. In the case of elongation the angles for pairs 12, 34 are smaller than those for the other pairs:

$$\theta_{12} = \theta_{34} \text{ in} < \theta_{13} = \theta_{14} = \theta_{23} = \theta_{24} \text{ out} \quad (2)$$

Typical values for in-plane,  $\theta_{\text{in}}$ , and interplane,  $\theta_{\text{out}}$ , angles calculated from geometrical considerations for some MnTe/ZnTe superlattices are listed in Table II. In the last two columns of the Table we give the values of the exchange constants calculated from Eq.(1). It can be easily seen that NN exchange interaction favors AFM ordering for the atoms within (001) plane. At the same time, the bonds between the atoms in neighboring planes are still equivalent and so are frustrated.

Further deformation within (001) plane (see Fig. 4 a, b) leads to optimization of the exchange in the interplane FM and AFM bonds by strengthening exchange interactions with the "right" sign and weakening those with the

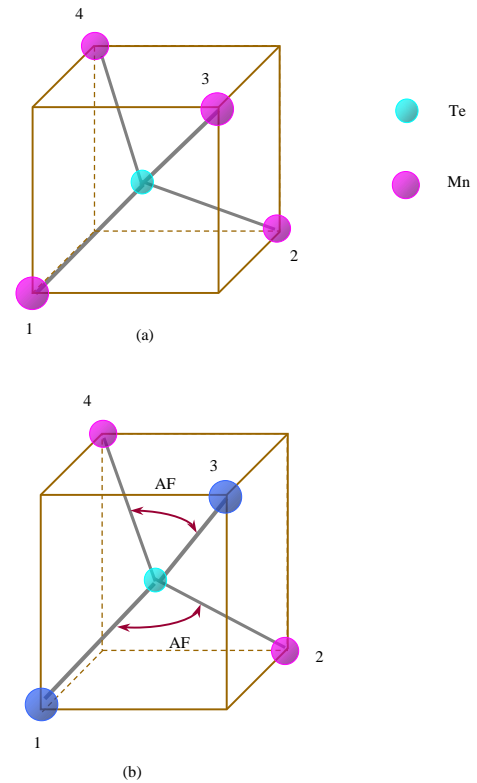


Figure 3: (Color online) Effect of the mismatch-induced stresses. Blue (1, 3) and magenta (2, 4) spheres correspond to Mn atoms with opposite directions of magnetization. (a) Nondeformed (cubic) cell, atoms in 1-4 positions are equivalent and angles between all the Mn-Te bonds are the same and equal  $109.5^\circ$ . (b) Elongation in [001] direction removes degeneracy between angles.

"wrong" sign. Namely, elongation in [100] direction (corresponding strain component  $u_{xx} - u_{yy} > 0$ ) results in

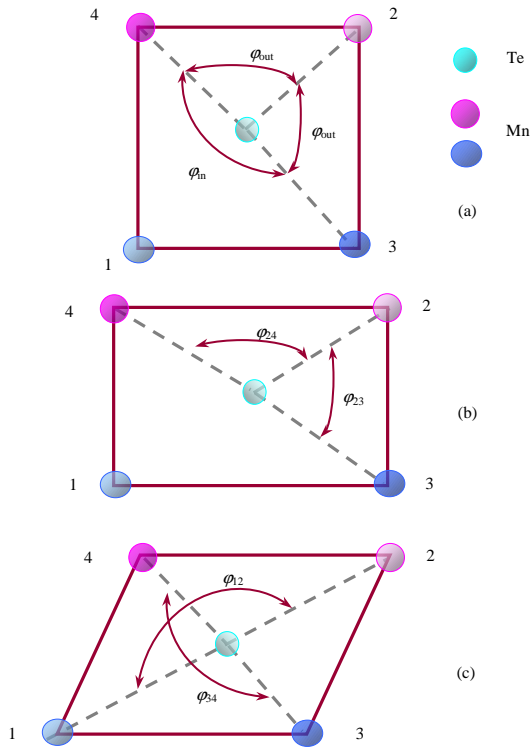


Figure 4: (Color online) Magnetostriiction in (001) plane. Pairs of antiferromagnetically coupled Mn atoms 1, 2 (hollow) and 3, 4 (filled) belong to different atomic planes. (a) Non-deformed state, angles between Mn-Te-Mn bonds take only two different values:  $\varphi_{in}$  (pairs 12 and 34) and  $\varphi_{out}$  (pairs 13, 14, 23 and 24). (b) Elongation in [100] direction removes degeneracy between the angles  $\varphi_{13} = \varphi_{24} > \varphi_{out} > \varphi_{23} = \varphi_{14}$ . (c) Shear strain  $u_{xy}$  removes degeneracy between the angles  $\varphi_{12}$  and  $\varphi_{34}$ .

the following difference between the exchange constants

$$J_{dd}(14) - J_{dd}(13) = \frac{0.27a_{xy}}{a_{xy}^2 + c^2} (u_{xx} - u_{yy}); K; \quad (3)$$

where  $a_{xy}$  and  $c$  are in-plane and interplane lattice parameters, correspondingly.

Thus, magnetostriiction can stabilize an AFM-III structure even in approximation of NN exchange interactions. On the other hand, magnetostriiction plays an important role in formation of ferroelectric ordering, as we will show below.

In the case of strong spin-orbit coupling some components of magnetostriictive tensor could depend upon the mutual orientation of a localized magnetic moment and a direction of anion-cation bond. This situation in application to MnTe is illustrated in Figs. 4c, 5. Shear strain  $u_{xy}$  in (001) plane makes AFM bonds between 1-2 and 3-4 pair inequivalent:

$$\varphi_{12} - \varphi_{34} = \frac{P}{c} \frac{2a_{xy} - 3c^2}{2a_{xy}^2 + c^2} 2a_{xy}^{-2} u_{xy} \approx 0.6u_{xy}; \quad (4)$$

The displacement  $\delta$  between the positive ( $Mn^{2+}$ ) and negative ( $Te^{2-}$ ) ions is thereby equal to

$$\delta = \frac{a_{xy}}{9} \frac{P}{2} u_{xy}; \quad (5)$$

For the totally ionic bond (with the effective charge  $2e$ ) and spontaneous strain  $u_{xy} = 3 \cdot 10^{-3}$  such a displacement induces a local dipole moment  $\approx 0.12$  D. Accurate calculations of ferroelectric polarization induced by spontaneous magnetostriction will be given in the next Sec. IV.

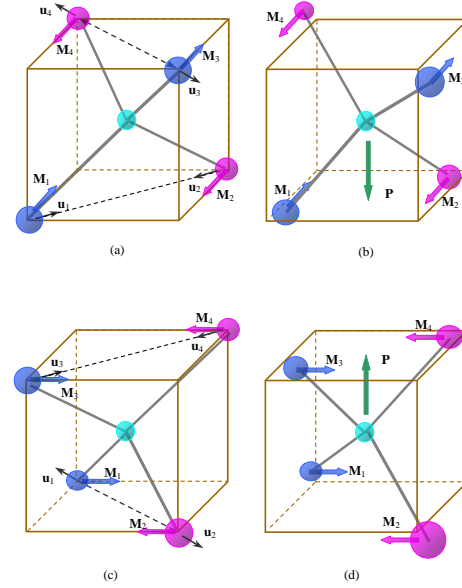


Figure 5: (Color online) Two types of AFM (and ferroelectric) domains. (a), (c) Mutual orientation of the sublattice magnetization (vectors  $M_j$ ,  $j = \overline{1,4}$ ) and shift vector ( $u_j$ ,  $j = \overline{1,4}$ ) of Mn atom. (b), (d) Arrangement of atoms after the shear strain. Non-equivalence of 1-2 and 3-4 bonds results in appearance of ferroelectric polarization  $P$ .

Fig. 5 reveals one interesting feature of the tetragonally distorted MnTe system: AFM structure can be implemented in two types of domains that have different (perpendicular) orientation of local magnetic moments (with respect to crystal axes) and opposite direction of electric polarization. AFM domains are clamped with ferroelectric ones. This means that macroscopic state of a sample can be controlled by application of either magnetic or electric field (or both). Behavior of the domain structure in the presence of the external fields will be discussed in Sec. V.

#### IV. POLARIZATION INDUCED BY AFM ORDERING: MODEL AND CALCULATIONS

Formally, AFM type-III structure can be described by the following distribution of magnetization vectors  $M(r_j)$

Table II: Angles between Mn-Te-Mn bonds for in-plane NN ( $\theta_{in}$ ) and interplane NN ( $\theta_{out}$ ) and corresponding values of exchange integrals  $J_{dd}(\theta_{in})$ ,  $J_{dd}(\theta_{out})$  (K) calculated from geometrical considerations for different superlattices. In-plane,  $a_{xy}$ , and interplane,  $c$ , lattice parameters (Å) are taken from the experimental paper Ref.23.

Type	$a_{xy}$	$c$	$\theta_{in}$	$\theta_{out}$	$J_{dd}(\theta_{in})$	$J_{dd}(\theta_{out})$
MnTe10/ZnTe18	6.130	6.570	105.7	111.4	-3.20	-3.97
MnTe20/ZnTe18	6.183	6.505	106.7	110.9	-3.27	-3.84
MnTe130/ZnTe330	6.150	6.470	106.7	110.9	-3.28	-3.83
MnTe	6.346	6.346	109.5	109.5	-3.45	-3.45

at Mn sites:

$$M(r_j) = L(q) \exp(iqr_j): \quad (6)$$

Three equivalent orientations of the structure vector  $q = (2/a; 0; a)$  (where  $a$  is a lattice constant), and two orientations of  $L$  vector (parallel to [100] and [010] axes) generate six types of AFM domains in MnTe. MnTe multilayers reduce de-

generacy to two possible domain types with the same  $q$  and mutually perpendicular  $L$  vectors in the  $lm$  plane.<sup>38</sup>

In a single-domain sample with the fixed magnetic order parameter (or AFM vector)  $L$  the equilibrium values of magnetostriction tensor,  $u$ , and electrical polarization,  $P$ , can be calculated by minimization of the following expression for the free energy

$$F = \int dV [ \frac{1}{2} (u_{xx}^2 + u_{yy}^2) + 2c_{16} u_{xy} ] (L_x^2 + L_y^2) (z) + \frac{1}{2} u_{ij} c_{ijkl} u_{kl} + \frac{P^2}{2\epsilon_0} + \frac{2e_{14}(z)}{\epsilon_0} (P_x u_{yz} + P_y u_{zx} + P_z u_{xy}) g \quad (7)$$

constructed from symmetry considerations. Parameters are magnetoelastic constants related to the shear strain,  $c$  is a tensor of the elastic modulus characteristic to cubic structure. Electrical properties are described by low-frequency dielectric constant  $\epsilon_{pm} = \epsilon_0 + 1$  and piezoelectric coefficient  $e_{14}$ ,  $\epsilon_0$  is the vacuum permittivity. Periodical alteration of the AFM (MnTe) and nonmagnetic (ZnTe) layers in a heterostructure is described by a form-function  $g(z)$  which equals 1 in AFM layer and vanishes in a nonmagnetic spacer.

In the case of ideal interfaces the strain induced by AFM ordering is homogeneous throughout the AFM and nonmagnetic layers and thus depends on the ratio of AFM layer thickness  $d$  to the period of superstructure  $D$ . In particular, macroscopic shear strain component  $u_{xy}$  which is responsible for polarization effect is given by the following expression

$$u_{xy}^{(sp on)} = \frac{16M_0^2}{2c_{44}} \frac{d}{D}; \quad (8)$$

where  $M_0 = 1$  distinguish between two orthogonal orientations of  $L$  k [100] and [010] in different domains,  $M_0 = \frac{1}{2} j_j$  is sublattice magnetization.

Strain-induced contribution<sup>49</sup> into spontaneous polarization calculated from (7), (8) is

$$P_z^{(sp on)} = 2e_{14} u_{xy}^{(sp on)} = \frac{e_{14}}{c_{44}} \frac{16M_0^2}{D} \frac{d}{D}; \quad (9)$$

For the multilayered structure the piezoelectric coefficient  $e_{14}(z)$  should be averaged over the AFM/NM bilayer.

It can be easily seen from the Expr. (9) that the direction of vector  $P$  correlates with that of AFM vector  $L$  (factor  $g$ ) and takes an opposite direction in the domains with  $L$  k [100] and [010], in accordance with intuitive predictions given above (see Fig. 5). So, coupling between the ferroelectric and antiferromagnetic order is accomplished by the rigid alignment of the antiferromagnetic axis perpendicular to the polarization direction.

Characteristic value of the spontaneous ferroelectric polarization in a single-domain state can be evaluated from (9) and available experimental data (see Table V II) as  $P^{(sp on)} = 60$  nC/cm<sup>2</sup>. For the thick MnTe  $P^{(sp on)}$  can be even higher because Mn atoms cause an enhancement of electromechanical coupling in zinc-blende structures.<sup>39</sup> It is remarkable that among the materials with comparable ferroelectric polarization (see Table I) MnTe shows the highest Neel temperature.

The value of the internal electric field  $E^{(sp on)} = 80$  kV/cm corresponding to the spontaneous polarization of MnTe is, in turn, close to strain-generated electric field in nonmagnetic III-V heterostructures.<sup>40</sup> It seems to be large enough to be detected due to the change in the photoluminescence spectra, like it was done in the Ref. 20.

V. SWITCHING OF POLARIZATION BY EXTERNAL MAGNETIC/ELECTRIC FIELD

Practical applications of multiferroics in information technology are based on their ability to maintain single ferroelectric domain state for a long time and change it under application of the external field. This can be achieved, for example, by using materials with a high ferroelectric Curie temperature and a robust large polarization (say,  $\text{RMnO}_3$ ,  $R = \text{Sc, Y, In, Ho}$  {Lu, see Refs. 41,42}) that, in turn, gives rise to a large value of switching field. In the systems with strong coupling between polarization and AFM order a single domain state can be easily fixed by a proper choice of the sample shape, even for small polarization. Moreover, if AFM and ferroelectric domains are intimately related and match up spatially (as, e.g., should be in MnTe), electric polarization of the sample can be switched by either magnetic or electric field. In this section we analyze field dependence of macroscopic polarization for different sample shapes.

Existence of equilibrium domain structure in the ferroics is usually attributed to the presence of long-range dipole-dipole interactions between the physically small ordered regions of the sample. Quantitative description of the phenomena is based on the account of shape-dependent contribution (stray energy) into free energy of the sample. In the case of ferroelectric (or ferromagnetic) materials this contribution can be written as

$$f_e = \frac{V}{2} h_{jp}^{(mag)} i @_{jkpt} h_{kt}^{(mag)} i^0; \quad (10)$$

where brackets  $h_{jkpt}$  mean averaging over the sample volume  $V$  and  $N$  is the second-rank depolarization tensor the components of which depend upon the shape of the sample.

Equilibrium domain structure in AFM with nonzero magnetoelastic coupling can be described in a similar way. Long-range (destressing) effects originate from the local internal stress fields  $h_{jk}^{(mag)}$  induced by magnetic ordering.<sup>43,44</sup> Corresponding contribution into free energy of the sample takes a form

$$f_{destr} = \frac{V}{2} h_{jp}^{(mag)} i @_{jkpt} h_{kt}^{(mag)} i^0; \quad (11)$$

where  $@_{jkpt}$  is the fourth-rank destressing tensor which, like  $N$ , depends upon the sample shape.

It was already mentioned that the domain structure of MnTe/ZnTe multilayers is formed by two (out of six) types of the domains with (i) Lk [100], Pk [001], volume fraction  $\beta$ , and (ii) Lk [010], Pk [00 $\bar{1}$ ], volume fraction  $(1 - \beta)$ . Switching between this two types can be performed by application of the external electric field  $E$  parallel to [001] axis or by the magnetic field  $H$  directed along one of the "easy" AFM axes ([100] or [010]).

In the most practical applications<sup>50</sup> macroscopic properties (such as polarization or elongation) of the multidomain sample depend on the single parameter  $\theta$  that can be calculated from minimization of shape-dependent ( $f_e + f_{destr}$ ) and field-dependent contributions into free energy:

$$\theta = V \left( S_1 E_z P_z^{(spon)} - \frac{d}{2D} H_y^2 \right) H_x^2 = \frac{1}{2} + \frac{1}{2} S_2 \frac{1}{2} : \quad (12)$$

Here spontaneous polarization  $P_z^{(spon)}$  within a domain is defined by the expression (9),  $\beta$  is the magnetic susceptibility of MnTe and  $S_{1,2}$  are shape-dependent coefficients<sup>51</sup>:

$$\begin{aligned} S_1 &= M_0^2 \langle \sigma_{11} \sigma_{22} \rangle; \\ S_2 &= 4N_3 P_z^{(spon)2} \\ &+ M_0^4 [(\sigma_{11}^2 + \sigma_{22}^2 - 2\sigma_{12}) + 16 \sigma_{16} \sigma_{66}]; \end{aligned} \quad (13)$$

where  $\langle \sigma_{xx} \rangle = \langle \sigma_{yy} \rangle$  are isotropic stresses induced in the  $lm$  plane due to the lattice mismatch.

A analysis of Eq.(12) shows that a single domain state of a sample ( $\theta = 1$  or  $0$ ) can be achieved either by the proper choice of the shape ( $2S_1 = S_2$ ) or application of the external field ( $E = E_{MD}$  or  $H = H_{MD}$ ) where we've introduced characteristic domainization fields

as follows:

$$E_{MD} = \frac{S_2}{2P_z^{(spon)}}; \quad H_{MD} = \frac{S_2 D}{d}; \quad (14)$$

In the multidomain state macroscopic ferroelectric polarization depends upon the external fields in a following way

$$h_{zi} = P_z^{(spon)} \frac{2S_1}{S_2} \frac{E_z}{E_{MD}} \frac{H_y^2 H_x^2}{H_{MD}^2} : \quad (15)$$

Let us analyze the properties of the coefficients  $S_{1,2}$  assuming that i) the sample has the shape of an ellipse (with semiaxes  $a, b$  and eccentricity  $k = \sqrt{1 - b^2/a^2}$ ) within the  $lm$  plane,  $lm$  thickness is  $h$ ; ii) elastic properties of the material are isotropic ( $c_{11} - c_{12} = 2c_{44}$ ) and are characterized with the shear modulus  $c_{44}$  and Poisson

ratio  $\epsilon_2 = (\epsilon_{11} + \epsilon_{12})$ . The destressing and depolarizing coefficients can be calculated explicitly in two limiting cases:

i) "pillar" with  $h > b$ :

$$S_1 = \frac{(\epsilon_{11} - \epsilon_{12}) d^2 M_0^2}{2c_{44} D (1 + \frac{k^2}{1 - k^2})^2};$$

$$S_2 = \frac{M_0^4 d^2}{2c_{44} D^2} (\epsilon_{11}^2 + 4 \frac{\epsilon_{12}^2}{16}) + \frac{4 \frac{\epsilon_{12}^2}{16} (\epsilon_{11}^2)}{1} \frac{k^4}{(1 + \frac{k^2}{1 - k^2})^4}; \quad (16)$$

ii) "thin film" with  $h < a$ :

$$S_1 = \frac{h}{b} \frac{(\epsilon_{11} - \epsilon_{12}) M_0^2 d}{4c_{44} (1 - k^2) D} J_2(k);$$

$$S_2 = \frac{4}{0} P_z^{(sp on)}{}^2; \quad (17)$$

where the dimensionless shape-factor is given by an integral

$$J_2(k) = \int_0^{\pi/2} \frac{(\sin^2 \theta + \cos^2 \theta k^2) d}{1 - k^2 \sin^2 \theta} d\theta$$

$$\begin{cases} 3 k^2 = 16; & k \neq 0 \\ 1; & k \neq 1; \end{cases} \quad (18)$$

It is remarkable that coefficient  $S_2$  that favors formation of the domain structure is nonzero in both limiting cases, as can be seen from (13), (16), (17). This fact can be easily extended to any geometry. Really, all the depolarizing effects (stray fields) are related with the flux of the corresponding (ferroelectric, magnetoelastic, etc) dipole moment through the sample surface. In our case the flux of ferroelectric polarization is nonzero only through the surface parallel to the film plane, thus "thin film" shows strong depolarizing ferroelectric effect while "pillar" shows none. In turn, AFM ordering produces stress dipoles within the film plane, so, corresponding flux is maximal through the side faces. As a result, strong destressing effect should be observed for the "pillar", not for the "thin film". For the intermediate case of the sample with the developed side and face surfaces ("ball" or "cube") coefficient  $S_2$  is contributed by both depolarizing mechanisms and so is nonvanishing for any shape.

Calculations based on the formulas (16), (17) and experimental data from Table VII show that in the case of MnTe multiferroic the destressing effects are much stronger ( $S_2 \approx 10^6 \text{ J/m}^3$ ) that the electric depolarization ( $S_2 \approx 5 \times 10^7 \text{ J/m}^3$ ), so, monodomination can be easier achieved in the "thin film".

Another interesting feature of the destressing phenomena is existence of the effective internal shape-induced field described by coefficient  $S_1$ . It arises due to cross-correlation between isotropic (induced either by substrate or by magnetovolume effect) and anisotropic internal stresses and has no analog in ferromagnetic or ferroelectric materials. Coefficient  $S_1$ , as seen from (16),

(17), (18), depends upon the eccentricity  $k$  and vanishes for the samples isotropic within the film plane ( $a = b$ ).

So, we can deduce that the shape of the sample influences the domain structure in two ways. First, the field of monodomination (14) strongly depends upon the  $h=b$  ratio. Characteristic values of the electric and magnetic monodomination fields for two limiting cases ( $h > b$  and  $h < b$ ) are given in Table VII. The value of  $H_{MD}$  for the thick sample ("pillar") is close to the value of anisotropy field 3.25 T (see Ref.45) and diminishes down to 0.8 T for "thin film".

Second, single domain state is energetically favorable for the samples with the overcritical eccentricity (calculated from the condition  $2S_1 = S_2$ ). For example, for the thick sample the critical eccentricity is 0.57 (corresponding aspect ratio  $a=b = 1.22$ ).

Shape effects are clearly seen in Fig. 6 which shows field dependence of macroscopic ferroelectric polarization for the "thin film" with  $h=b = 0.1$  and for the "pillar", both samples having the same in-plane eccentricity 0.1 (corresponding aspect ratio  $a=b = 1.005$ ). In the first case monodomination field is smaller and biasing effect is more pronounced.

Monodomination of the sample can be also achieved by the combined application of the electric and magnetic field, as illustrated in Fig. 7 for the case of "thin film" with zero eccentricity. Relation between the switching fields in this case is given by the formula

$$\frac{E_z}{E_{MD}} + \frac{H_y^2 - H_x^2}{H_{MD}^2} = 1; \quad (19)$$

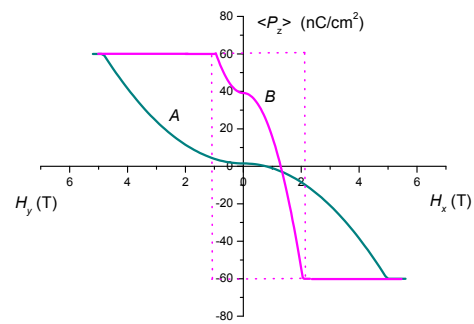


Figure 6: (Color online) Macroscopic ferroelectric polarization as a function of external magnetic field calculated according to (15) for "thin film" with  $h=b = 0.1$  (curve A, magenta) and "pillar" (curve B, dark cyan). The eccentricity in both cases is  $k = 0.1$ . Magnetic field  $H$  is switched between  $x$  and  $y$  directions. Dotted curve (magenta) shows the possible field switching between two opposite polarizations in a single domain sample.

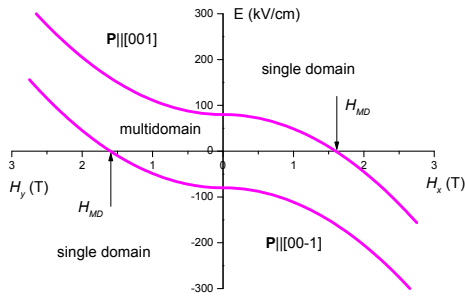


Figure 7: (Color online) Phase diagram in  $E$ - $H$  variables for the thin film ( $h=b=0.1$ ) with zero eccentricity. Magnetic field  $H$  is switched between  $x$  and  $y$  directions.

## V I. VISUALIZATION OF THE DOMAIN STRUCTURE

The zinc-blend wide-gap semiconductors are also known to show nonlinear optical properties studied in second harmonic generation (SHG) experiments.<sup>46</sup> In the paramagnetic phase these crystals have the only nonzero SHG tensor component  $d_{14}$  ( $d_{25}; d_{36}$ ) which is rather large, e.g. for ZnTe it is 119 pm/V at the fundamental wavelength 1047 nm.<sup>46</sup> AFM ordering may bring to being additional SHG components. To calculate them we analyze the response to the external electric field with account of the nonlinear contribution into free energy

$$F^{(\text{nonlin})} = \frac{2d_{14}}{2} P_x P_y P_z + \frac{0}{2} (P_x^2 - P_y^2) (u_{xx} - u_{yy}) + \frac{2}{0} (P_x P_y u_{xy} + P_y P_z u_{yz} + P_z P_x u_{zx}) + (z) [1 (M_x^2 + M_y^2) P_z (P_x^2 - P_y^2) + 2 (M_x^2 - M_y^2) P_z^3]; \quad (20)$$

Coefficients  $d_{14}$ ,  $d_{44}$  introduced in (20) describe electrostrictive effect and the last term describes high-order magneto-electric coupling.

Calculations show that in the AFM phase the crystal becomes biaxial with anisotropic dielectric tensor:

$$\begin{aligned} \epsilon_{xx} = \epsilon_{zz} = \epsilon_{yy} &= \frac{0}{c_0} M_0^2 (p_m \pm 1); \\ \epsilon_{xy} &= \frac{44}{C_{44}} M_0^2 (p_m \pm 1); \end{aligned} \quad (21)$$

in accordance to symmetry prediction for  $C_2$  point group of AFM phase. The SHG tensor components proportional to AFM vector are of two types. Like dielectric coefficients, the components

$$d_{31} + d_{32} = \frac{4}{C_{44}} d_{14} M_0^2 = 2u_{xy}^{(\text{sp on})} d_{14}; \quad (22)$$

have opposite signs for the domains with perpendicular orientation of AFM vectors ( $\pm = 1$ ). The other coefficients are insensitive to the domain structure:

$$\begin{aligned} d_{24} = d_{5} &= \frac{1}{2} (d_{32} - d_{31}) = M_0^2 \frac{1}{2} (p_m (\pm) \pm 1); \\ d_{33} &= M_0^2 \frac{2}{0} (p_m (\pm) \pm 1); \end{aligned} \quad (23)$$

The symmetry predicted difference between the  $d_{14}$ ,  $d_{25}$  and  $d_{36}$  components is due to the high-order terms in the magnetic order parameter and is neglected.

Rotation of the polarization plane which may stem from anisotropy of dielectric tensor and effect of SHG are sensitive to the direction of AFM vector and thus open a possibility to visualize the AFM domain pattern.<sup>26</sup>

## V II. SUMMARY AND CONCLUSIONS

In the present paper we demonstrate for the first time that MnTe epitaxial films and MnTe/ZnTe multilayers grown in a convenient (001)-direction should become electrically polarized below the Neel temperature. Spontaneous ferroelectric polarization results from the bending of highly ionic Mn-Te-Mn bonds induced by magnetostrictive shear strain.

In contrast to many other multiferroics, MnTe has no macroscopic magnetic moment and the direction of ferroelectric polarization is coupled with the orientation of AFM order parameter. Thus, the domain structure is formed by the combining action of the electric and magnetoelastic dipole-dipole interactions. Corresponding depolarizing long-range contribution into free energy of the sample is nonzero for any sample shape. In the case of thick film depolarizing effects are governed mainly by magnetoelastic mechanism and corresponding monodomainization field is of the same order as characteristic anisotropy field. In the case of thin film depolarization is due to the presence of the electric dipole interactions and corresponding monodomainization field is much smaller.

Due to the clamping between the electrical and AFM domains switching between the opposite direction of ferroelectric polarization can be induced by application of the magnetic field parallel to "easy" AFM axis. Vice versa, one can switch between different (100-oriented and [010]-oriented AFM domains) by application of the electric field. This effect seems to be useful for controlling the state of the adjacent ferromagnetic layer coupled to the multiferroic through exchange interactions like it was proposed in Ref.9.



AFM ordering may also induce additional (anisotropy) components of dielectric and SHG tensors. The sign of the effect is sensitive to orientation of AFM vectors and thus opens a possibility to distinguish different domain types. The spontaneous ferroelectric effect is peculiar to the collinear AFM – III ordering and is not allowed (from symmetry point of view) in the canted AFM – III structure (e.g., such an effect is impossible in MnTe/CdTe multilayers).

Acknowledgments

H.G. would like to acknowledge Prof. P. Bruno for fruitful discussions. This work is supported partly by State Foundation for Fundamental Researches of Ukraine and partly by Ministry of Science and Education of Ukraine

- Electronic address: malyshen@ukrpack.net; Bogolyubov Institute for Theoretical Physics NAS of Ukraine, Metrologichna str. 14-b, 03143, Kyiv, Ukraine
- <sup>1</sup> T. Kinoshita, S. Kawamoto, I. Yamada, M. Azuma, M. Takano, and Y. Tokura, *Phys. Rev. B* **67**, 180401 (2003).
  - <sup>2</sup> J. Henberger, P. Lunkenheimer, R. Fichtl, H. A. K. von Nida, V. Tsurkan, and A. Loidl, *Nature* **434**, 364 (2005).
  - <sup>3</sup> M. Gajek, M. Bibes, S. Fusil, K. Bouzehouane, J. Fontcuberta, A. Barthelémy, and A. Fert, *Nat. Mater.* **6**, 296 (2007).
  - <sup>4</sup> H. Wiegmann, I. M. Vitelsky, A. A. Stepanov, A. G. M. Jansen, and P. Wyder, *Phys. Rev. B* **55**, 15304 (1997).
  - <sup>5</sup> T. Lottermoser, T. Lonkai, U. Amann, D. Hohlwein, J. Ihlinger, and M. Fiebig, *Nature (London)* **430**, 541 (2004).
  - <sup>6</sup> J. Baier, D. Meier, K. Berggold, J. Henberger, A. Balbashov, J. A. Mydosh, and T. Lorenz, *Phys. Rev. B* **73**, 100402 (2006).
  - <sup>7</sup> B. Kundys, C. Simon, and C. Martin, *Phys. Rev. B* **77**, 172402 (2008).
  - <sup>8</sup> J. Okamoto, D. J. Huang, C. Y. Mou, K. S. Chao, H. J. Lin, S. Park, S.-W. Cheong, and C. T. Chen, *cond-mat/0703234* (2007).
  - <sup>9</sup> Y.-H. Chu, L. W. Martin, M. B. Holcomb, and R. Ramesh, *Materials Today* **10**, 16 (2007).
  - <sup>10</sup> D. I. K. Jeroen van den Brink, *arXiv:0803.2964v2* (2008).
  - <sup>11</sup> K. Morishita, K. Iio, T. Mitsui, and T. Kato, *JM M* **226**, 579 (2001).
  - <sup>12</sup> I. Komev, M. Bichurin, J. P. Rivera, S. Gentil, H. Schmid, A. G. M. Jansen, and P. Wyder, *Phys. Rev. B* **62**, 12247 (2000).
  - <sup>13</sup> M. Fiebig, D. Froehlich, S. Leute, and R. V. Pisarev, *Appl. Phys. B* **66**, 265 (1998).
  - <sup>14</sup> A. B. Sushkov, M. Mostovoy, R. V. Aguilar, S.-W. Cheong, and H. D. Drew, *J. Phys. C* **20**, 434210 (2008).
  - <sup>15</sup> I. A. Sergienko and E. Dagotto, *Phys. Rev. B* **73**, 094434 (2006).
  - <sup>16</sup> C. D. Hu, *Phys. Rev. B* **77**, 174418 (2008).
  - <sup>17</sup> L. C. Chapon, P. G. Radaelli, G. R. Blake, S. Park, and S.-W. Cheong, *Phys. Rev. Lett.* **96**, 097601 (2006).
  - <sup>18</sup> J. K. Furdyna, *J. Appl. Phys.* **64**, R29 (1988).
  - <sup>19</sup> J. L. Pautrat, *J. Phys. III (Paris)* **12**, 2413 (1994).
  - <sup>20</sup> R. Andre, C. D. Eshayes, J. Cibert, L. S. Dang, S. Tatarenko, and K. Saminadayar, *Phys. Rev. B* **42**, 11392 (1990).
  - <sup>21</sup> B. E. Larson, K. C. Hass, H. Ehrenreich, and A. E. Carlson, *Phys. Rev. B* **37**, 4137 (1988).
  - <sup>22</sup> H. Krenn, R. Rupprecht, S. Holl, W. Faschinger, H. Pascher, and G. Bauer, *Physica B* **256–258**, 548 (1998).
  - <sup>23</sup> T. M. Giebultowicz, P. Kłosowski, N. Samarth, H. Luo, J. K. Furdyna, and J. J. Rhyne, *Phys. Rev. B* **48**, 12817 (1993).
  - <sup>24</sup> B. Hennion, W. Szuszkiewicz, E. Dynowska, E. Janik, and T. Wojtowicz, *Phys. Rev. B* **66**, 224426 (2002).
  - <sup>25</sup> T. M. Giebultowicz, H. Kępa, J. Blinowski, and P. Kacmian, *Physica E* **10**, 411 (2001).
  - <sup>26</sup> M. Fiebig, T. Lottermoser, D. Frohlich, A. V. Goltsev, and R. V. Pisarev, *Nature (London)* **419**, 818(820) (2002).
  - <sup>27</sup> M. Fiebig, *J. Phys. D* **38**, R123 (2005).
  - <sup>28</sup> B. Kundys, A. Maignan, C. Martin, N. Nguyen, and C. Simon, *arXiv.org:0802.2877* (2008).
  - <sup>29</sup> D. Higashiyama, S. Miyasaka, N. Kida, T. Arima, and Y. Tokura, *Phys. Rev. B* **70**, 174405 (2004).
  - <sup>30</sup> C. R. delacruz, B. Lorenz, Y. Y. Sun, C. W. Chu, S. Park, and S.-W. Cheong, *Physical Review B (Condensed Matter and Materials Physics)* **74**, 180402 (2006).
  - <sup>31</sup> Y. Yamasaki, H. Sagayama, T. Goto, M. Matsuura, K. Hirota, T. Arima, and Y. Tokura, *cond-mat/0701430* (2007).
  - <sup>32</sup> G. Lawes, A. B. Harris, T. Kinoshita, N. Rogado, R. J. Cava, A. Aharony, O. Entin-Wohlman, T. Yildirim, M. Kenzelmann, C. Broholm, et al., *Physical Review Letters* **95**, 087205 (2005).
  - <sup>33</sup> P. Khare, C. Sudakar, A. B. Harris, R. Naik, and G. Lawes, *arXiv.org:0711.4137* (2007).
  - <sup>34</sup> H. Wu, T. Bumus, Z. Hu, C. Martin, A. Maignan, J. C. Cezar, A. Tanaka, N. B. Brookes, D. I. Khomskii, and L. H. Tjeng, *arXiv:0806.1607v1* (2008).
  - <sup>35</sup> T. M. Giebultowicz, H. Luo, N. Samarth, J. K. Furdyna, and J. J. Rhyne, *IEEE Trans. Magn.* **29**, 3382 (1993).
  - <sup>36</sup> R. Rupprecht, H. Pascher, H. Krenn, W. Faschinger, and G. Bauer, *Phys. Rev. B* **63**, 115325 (2001).
  - <sup>37</sup> A. Bruno and J. P. Lascaray, *Phys. Rev. B* **38**, 9168 (1988).
  - <sup>38</sup> H. Gomony, *Phys. Rev. B* **64**, 054404 (2001).
  - <sup>39</sup> P. Maheswaranathan and R. J. Sladek, *Phys. Rev. B* **31**, 7910 (1985).
  - <sup>40</sup> D. L. Smith, *Microelectronics Journ.* **28**, 707 (1997).
  - <sup>41</sup> M. Fiebig, *Phase Transitions* **79**, 947 (2006).
  - <sup>42</sup> N. Hur, I. K. Jeong, M. F. Hundley, S. B. Kim, and S.-W. Cheong, *arXiv:0805.3289v1* (2008).
  - <sup>43</sup> E. Gomony and V. M. Loktev, *J. Phys. C* **14**, 3959 (2002).
  - <sup>44</sup> H. V. Gomony and V. M. Loktev, *Phys. Rev. B* **75**, 174439 (2007).
  - <sup>45</sup> R. Swirkowicz, *J. Phys. C* **12**, 2913 (2000).
  - <sup>46</sup> H. P. Wagner, M. Kuhnelt, W. Langbein, and J. M. Hvam, *Phys. Rev. B* **58**, 10494 (1998).
  - <sup>47</sup> A. Lewicki, J. S. and J. K. Furdyna, and R. R. Galazka, *Phys. Rev. B* **37**, 1860 (1988).
  - <sup>48</sup> Experiments of Hennion et al.<sup>24</sup> ruled out the existence of

Table III: Values of constants for MnTe (ZB) used in calculations and calculated (see text for notations).

Constant	Value	Source/formula	Rem.
$T_N$	65 K	Ref23	
$c=a$	1.06	Ref23	
$u_{xx}$ $u_{yy}$	0,003	Ref23	
$e_{14}$	0.097 C/m <sup>2</sup>	Ref39	Cd <sub>81</sub> Mn <sub>19</sub> Te
$p_m$	9,5	Ref39	
$C_{11}$	53.6 GPa	Ref39	Cd <sub>81</sub> Mn <sub>19</sub> Te
$C_{12}$	37 GPa	Ref39	Cd <sub>81</sub> Mn <sub>19</sub> Te
$C_{44}$	18.2 GPa	Ref39	Cd <sub>81</sub> Mn <sub>19</sub> Te
$M_0$	615 Gs	Ref21	
	$1.8 \cdot 10^4$ cgs	Ref47	T = 0
	0.41	$q_2 = (C_{11} + C_{12})$	
$u_{mf}$	0.03	$0.5(c=a-1)$	
$u_{mf}$	2.7 GPa	$(C_{11} + C_{12})u_{mf}$	
$M_0^2$	0.06 GPa	$C_{44}(u_{xx} - u_{yy})$	
$P_z^{(sp\text{on})}$	60 nC/cm <sup>2</sup>	(9)	
$E^{(sp\text{on})}$	80 kV/cm	$P_z^{(sp\text{on})} = (0)$	
$E_{MD}$	750 kV/cm	(14)	\pillar"
$E_{MD}$	40 kV/cm	(14)	\thin m "
$H_{MD}$	3.5 T	(14)	\pillar"
$H_{MD}$	0.8 T	(14)	\thin m "

anisotropic exchange mechanism in this system.

<sup>49</sup> The analogous contribution into polarization may also arise from the direct magneto-electric coupling omitted in the Expr.(7).

<sup>50</sup> For the ellipsoid-shaped samples disregarding small contribution from the domain walls and possible closure domains.)

<sup>51</sup> We use Voight notations for the components of the symmetric 2-nd and 4-th rank tensors